Cloud-based battery failure prediction and early warning using multi-source signals and machine learning

Zhang, Xiaoxi; Pan, Yongjun; Cao, Yangzheng; Liu, Binghe; Yu, Xinxin

DOI
10.1016/j.est.2024.112004

Publication date
2024

Document Version
Final published version

Published in
Journal of Energy Storage

Journal of Energy Storage 93 (2024) 112004

Contents lists available at ScienceDirect

Journal of Energy Storage

journal homepage: www.elsevier.com/locate/est

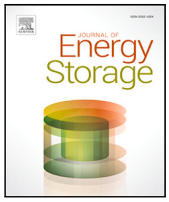

Research papers

Cloud-based battery failure prediction and early warning using multi-source signals and machine learning

Xiaoxi Zhang [a], Yongjun Pan [a,*], Yangzheng Cao [a], Binghe Liu [a,*], Xinxin Yu [b,c]

[a] State Key Laboratory of Mechanical Transmission for Advanced Equipments, College of Mechanical and Vehicle Engineering, Chongqing University, Chongqing, 400044, China

[b] Laboratory of Machine Design, Department of Mechanical Engineering, LUT University, Lappeenranta, Finland

[c] Section of Railway Engineering, Delft University of Technology, Delft, The Netherlands

ARTICLE INFO

Keywords:
Battery safety
Cloud-based
Machine learning
Failure mode recognition
Pre-short-circuit warning
Post-short-circuit prediction

ABSTRACT

The swift advancement of electric vehicle technology has led to increased requirements for ensuring the safety of batteries. Various models for predicting battery life and aging have been introduced to facilitate the appropriate utilization of batteries. Timely prediction and alert systems for identifying potential battery failure due to mechanical abuse are of utmost importance. The ongoing progress in machine learning (ML) algorithms and the evolution of extensive cloud-based models offer viable solutions for predicting and issuing early warnings for battery failure. This study focuses on a crucial aspect of EV safety: the timely prediction and prevention of battery failure caused by mechanical abuse. It introduces a cloud-based framework designed for the prediction and early detection of battery failure. The framework comprises three components, with the first being a model for recognizing failure modes resulting from mechanical abuse of batteries. To achieve this aim, a self-organizing map-back propagation (SOM-BP) model is employed, which integrates both supervised and unsupervised learning capabilities to identify three distinct failure conditions: bending, compression, and indentation. The second part involves the implementation of a prediction and pre-short-circuit warning. This is achieved through the utilization of whale optimization algorithm-support vector regression (WOA-SVR) and tuna swarm optimization-support vector regression (TSO-SVR) models to forecast the remaining duration until mechanical failure and short-circuit occurrence. Additionally, these models facilitate the prediction of voltage and temperature levels at the subsequent sampling time. The third part deals with the implementation of battery post-short-circuit prediction using WOA-SVR, TSO-SVR, and random forest models. This involves sampling the temperature, subsequent current, and voltage under various SOCs and then comparing the characteristics of the three models. The findings indicate that the ML models are capable of accurately identifying, predicting, and providing early warnings for failure modes. This work proposes a scalable and potentially efficient solution by leveraging cloud computing for data storage, processing, and model training. The collaboration between the cloud model and vehicle-side information can effectively ensure the safety of passengers.

1. Introduction

1.1. Research background

The popularity of electric vehicles has put forward higher requirements for battery safety [1–9]. The battery may experience deformation when subjected to mechanical abuse, leading to penetration of the separator and resulting in internal short-circuits. In more severe instances, thermal runaway may occur, potentially leading to fire or explosion. It will seriously endanger the lives of passengers and trigger a crisis of trust among consumers, so the safe design of batteries is of great importance [10–15].

Currently, numerous scholars have made significant contributions to the advancement of energy storage and battery technology [16–32]. Cao et al. developed a fully detailed three-dimensional expansion mechanics model of the battery and analyzed the expansion force and inhomogeneous stress distribution of each component [33]. Yan et al. proposed an evaluation method for series-connected battery systems based on fault distribution analysis, which can improve the service life by redundant batteries [34]. Shin et al. proposed a

* Corresponding authors.
E-mail addresses: yongjun.pan@cqu.edu.cn (Y. Pan), liubinghe@cqu.edu.cn (B. Liu).

https://doi.org/10.1016/j.est.2024.112004
Received 23 February 2024; Received in revised form 25 April 2024; Accepted 12 May 2024
Available online 30 May 2024

Nomenclature

U^{1D}	voltages of the 1D model
U^{St}	voltages of the short-circuit model
i^{1D}	current densities of the 1D model
i^{St}	current densities of the short-circuit model
B	coefficient characterizing the relationship between the 1D model and the short-circuit model
q^{1D}	heat production rate of the 1D battery model
q^{Tl}	loading heat rate of the 3D thermal model
T^{1D}	temperatures of the 1D battery model
T^{Tl}	average temperature of the 3D thermal model
q^{a}	reaction heat rate
q^{j}	joule heat rate
q^{r}	resistance heat rate from current collectors
q^{i}	irreversible heat rate
q^{Ta}	overall heat rate of the 3D thermal model
q^{St}	heat production rate of the short-circuit model
S^{St}	cross section
L^{Ng}	length of anode
L^{Ps}	length of cathode
$N^{St}(t)$	number of short-circuit parts in parallel
C	coefficient related to the geometrical parameters of the cell
x_k	normalized values
x_k^*	original values
$\min\left(x_k\right)$	minimum values
$\max\left(x_k\right)$	maximum values
$x(t)$	input vector
$w_i(t)$	weights in the competitive layer
$w_c(t)$	weight of the winning node
$\alpha(t)$	learning rate
d	Euclidean distance
$h_{ci}(t)$	neighborhood function value
$\mathbf{X^n}$	output value vector
$\mathbf{B^n}$	bias matrix of neurons
$\mathbf{W^n}$	weight matrix
$\mathbf{L}$	loss function
y_i	regression value
y	true value
a	acceptable deviation threshold
$\mathbf{W}$	normal vector
$\mathbf{b}$	intercept vector
$F_T(x)$	output of the random forest algorithm
T	number of decision trees
$D_t(x)$	output of the tth decision tree
ω_t	weight of different decision trees

methodology for modeling vehicle-grade lithium-ion batteries through vehicle chassis dynamometer testing, and these battery models can be adopted into electric vehicle models [35]. Yang et al. outlined the fundamentals of heat generation, accumulation, and transport in battery systems and highlighted recent key research on material design to improve the safety of sodium-ion batteries [36]. Zhang et al. proposed an early warning model based on an intelligent algorithm that can reliably identify the abnormal state of electric vehicle charging voltage and issue timely warnings [37]. Xia et al. used the LS-DYNA finite element program to establish a three-dimensional model for analyzing the impact response and fracture of polyurethane-coated aluminum panels, and discussed in detail the effects of polyurea stiffness, aluminum strength, adhesive strength, and polyurethane thickness on the impact resistance of polyurethane-coated aluminum panels, as well as analyzing the effects of staggered layout of the battery cells on mitigating the damage to the batteries [38,39]. Zhang et al. provide ideas for efficient forward and reverse mechanical safety design and multi-objective optimization design of battery pack systems using finite element method and intelligent algorithms [40,41].

Numerous researchers have made significant contributions to the study of battery degradation and the forecasting of battery SOH through the application of diverse algorithms [42–47]. Li et al. proposed a novel Gaussian process regression model based on partial incremental capacity curves, which can provide accurate and robust SOH estimation for batteries [48]. Xiong et al. realized the accurate voltage estimation for different battery aging degrees by the advanced time scale separation algorithm and obtained the accurate estimation of battery capacity and SOC in real-time [49]. Zhang et al. developed a novel physical feature-driven battery life prediction method for mobile windows, which can be used to predict the remaining battery life and knee point, and for the first time to classify the battery life in real-time [50]. Ying et al. examined the results of component tests performed on cells at different temperatures and health states, and the analysis showed that particles and adhesion had different effects on temperature effects and aging effects [51]. Park et al. consider battery aging management for electric vehicle batteries in the charging station operating environment from the perspective of a charge point operator, and analyze the technical and economic effects of battery aging management based on participation in electric service [52]. Barcellona et al. analyzed the variation rule of internal resistance with temperature and SOC under different aging conditions. They proposed a mathematical model to predict how the internal resistance of the battery varies with temperature, SOC, and aging using the results of the experiments [53].

1.2. Motivation and related work

Early warnings about battery safety are extremely important, and timely warnings can warn drivers and create more time to escape. Ongoing developments in sophisticated algorithms are providing increased opportunities for the implementation of early warning systems [54,55]. Nevertheless, the challenge lies in implementing early warnings due to the relatively stable voltage and current signals exhibited by batteries before a short-circuit event [56,57].

Huang et al. experimentally developed a predictive model for early detection of battery failure, integrating factors such as exhaust gas dispersion and thermal runaway. This model enables the anticipation of critical events in battery operation, including the initial discharge, thermal runaway occurrence, and gas flow rate, thereby serving as a valuable tool for preemptive identification of potential battery malfunctions [58]. Chen et al. conducted a study on the deformation mechanism of prismatic batteries during thermal runaways and proposed a method for detecting thermal runaways in batteries early by utilizing mechanical strain data [59]. Jindal et al. developed a computational model incorporating conjugate heat transfer, electrochemical, and abusive reaction kinetics to forecast the thermal runaway propagation characteristics of a cylindrical lithium-ion battery module. The model also establishes a dimensionless threshold for designing a cooling system to effectively mitigate thermal runaway incidents [60]. Maura C et al. introduced a novel approach for fault detection in batteries that does not depend on traditional electrical measurements such as voltage and current. Instead, their method utilizes ultrasound technology to directly assess the battery's condition by analyzing alterations in the material characteristics of its components. Additionally, the researchers

Table 1
Comparison of related studies.

Authors	Signal category	Methods	Application scenario
Huang et al. [58]	Gas signal	Gas sensor to obtain gas pressure	Thermal runaway
Chen et al. [59]	Strain signal	Strain gauges to obtain mechanical strain	Thermal runaway
Jindal et al. [60]	Electrochemical & heat signals	Multi-physics field coupling model	Thermal runaway
Maura C et al. [61]	Ultrasound signal	Ultrasound device detects ultrasound	Overcharging & failure
Xu et al. [62]	Electrical & heat signals	Evaluation of accident vehicle signals	Cell failure
This work	Mechanical & electrical & heat signals	Machine learning	Internal short-circuit

established two distinct alert modes aimed at issuing timely notifications in the event of overcharging or the presence of faults [61]. Xu et al. introduced a safety early warning model for electric vehicle power battery packs utilizing operational data. The model involves the extraction of voltage, temperature, internal resistance, and charge data from accident vehicles over two years. These four factors are utilized for evaluating the consistency of battery packs, with a focus on analyzing their variations during vehicle operation and before thermal runaway. This analysis aims to measure the extent of inconsistency within the packs and to pinpoint problematic cells through the application of two distinct evaluation techniques [62]. The comparison of these researches is presented in Table 1.

1.3. Contributions

Nevertheless, the robustness of the model can be challenged by using a single signal for predictive warnings. The utilization of multi-source signals, in conjunction with cloud-based large-scale models, has the potential to offer effective strategies for the early warning of battery failure. In this work, a cloud-based framework for battery failure prediction and early warning is presented. The framework consists of three parts, the first part is a failure mode recognition model for mechanical abuse of batteries, a self-organizing map-back propagation (SOM-BP) model that combines supervised and unsupervised learning features is utilized to identify three failure conditions: bending, compression, and indentation. The subsequent component involves the implementation of a prognostic and cautionary framework prior to a short-circuit event. This is achieved through the utilization of whale optimization algorithm-support vector regression (WOA-SVR) and tuna swarm optimization-support vector regression (TSO-SVR) models to forecast the remaining duration until mechanical failure and short-circuit occurrence. Additionally, these models facilitate the prediction of voltage and temperature levels at the subsequent sampling time. The third part is the post-short-circuit prediction model, WOA-SVR, TSO-SVR, and random forest (RF) model are utilized to predict the temperature of the battery after short-circuiting and sampling the subsequent current and voltage under different SOCs, and the features of the three models are compared. This method enables the deployment of models in cloud-based systems, facilitating the generation of predictive alerts through the integration of data from the cloud and the vehicle. This is aimed at safeguarding occupants in the event of battery mechanical abuse. The highlights of this work are summarized as follows:

- A novel method for recognizing failure modes was presented by integrating SOM model and BP model.
- A predict model was developed for the early warning of battery short-circuit.
- A novel model was provided to accurately forecast the variations in temperature, current, and voltage of different SOCs following a short-circuit.

The rest of this work is organized as follows. In Section 2, sources of data acquisition are described, and the underlying logic of multiphysics field modeling is presented. In Section 3, a model for recognizing failure modes was developed by integrating the characteristics of the unsupervised learning clustering model SOM with the supervised learning model BP. This combined model effectively identifies failure modes by analyzing mechanical signals. Specifically, the model successfully distinguishes between three modes – bending, compression, and indentation – based on battery forces, displacements, and force increments. In Section 4, a model was developed to forecast the time until mechanical failure and short-circuit occurrence in a battery, along with the anticipated voltage and temperature at the subsequent moment. Two forecasting models, WOA-SVR and TSO-SVR, were developed and evaluated for precision, with the findings indicating a remarkably high level of accuracy. In Section 5, a model for predicting battery short circuit events was developed to accurately forecast the variations in temperature, current, and voltage for various SOCs following a short circuit. Here, three prediction models, WOA-SVR, TSO-SVR & RF, are constructed to perform post-short-circuit prediction, and each model demonstrates different features. In Section 6, the work was concluded.

2. Cloud-based battery failure prediction and warning framework

In this section, a method for predicting battery failure using cloud-based data is introduced, along with an explanation of pattern recognition and the data sources utilized for the predictive warning model. In situations of mechanical abuse, the battery components sustain damage, causing the positive and negative materials within the battery to come into direct contact or connect with the conduction pathway. This contact results in the generation of current discharge due to the potential difference, leading to the release of a significant amount of heat. This phenomenon is commonly referred to as an internal short-circuit of the battery. The occurrence of a short-circuit within the battery causes energy to accumulate, which in turn triggers the breakdown of the internal structure of the battery. This breakdown may involve processes such as the decomposition of the solid electrolyte interphase film, reactions within the electrolyte, and decomposition of the positive electrode material. Ultimately, these events can culminate in thermal runaway, combustion, and even explosion. Real-time interaction between cloud data and vehicle-collected signal data can be used to identify the failure mode of the battery and predict the short-circuit time, temperature rise after the short-circuit, and voltage and current changes. The cloud-based security prediction and warning platform proposed in this paper consists of three components: failure mode recognition, pre-short-circuit warning, and post-short-circuit prediction, as shown in Fig. 1.

In the first phase, when the battery pack system collects anomalous mechanical data, it sends the anomalous data to the cloud platform and utilizes its large-scale model to identify patterns of mechanical abuse suffered by the battery. The failure scenarios for the three models are shown in Table 2. In the second stage, following the identification of the battery failure mode, the cloud platform leverages the real-time transmission of mechanical, voltage, and temperature anomaly data from the vehicle to forecast the voltage and temperature in the subsequent moment. It also warns about the mechanical failure time of the battery structure and the short-circuit time of the battery. During the third phase, in the event of a short circuit, the vehicle transmits current and voltage data to the cloud, which is then integrated with the SOC of the vehicle to forecast the battery's voltage, current, and temperature for the subsequent moment. This allows for the real-time prediction and warning of battery failure through cloud-based technology.

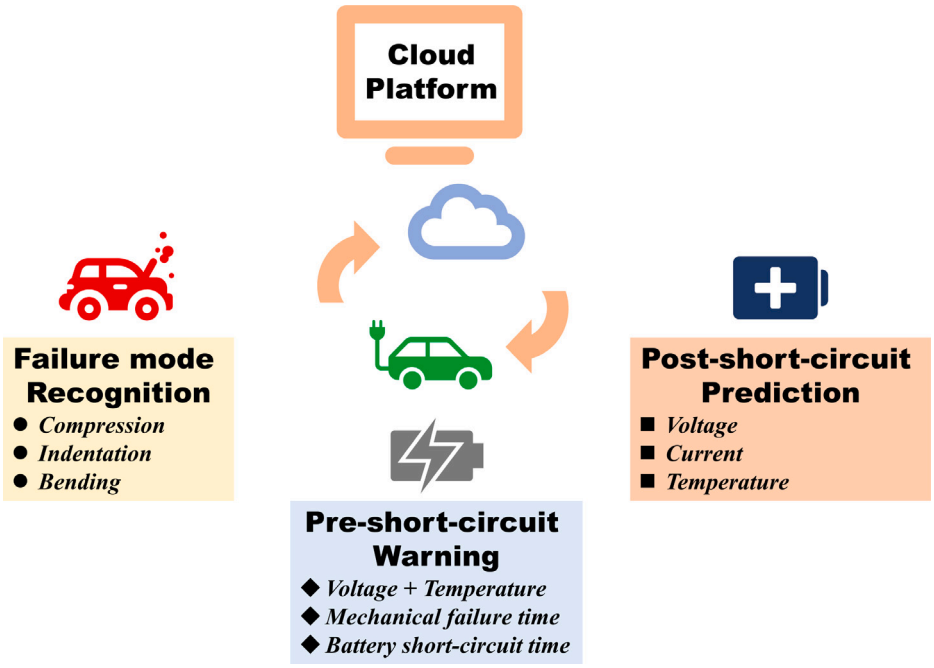

Fig. 1. The cloud-based security prediction and warning platform.

Table 2
Failure scenarios for the three modes.

Failure mode	Failure scenarios
Compression	Collision with large flat surfaces (wall, large boxes, etc.)
Bending	Medium-sized extrusion deformation (trees, utility poles, streetlights, etc.)
Indentation	Small size structure collision (stone, etc.)

A cloud-based predictive and alert system for battery failure was developed by acquiring datasets comprising force response, voltage and current, and temperature. These datasets were sourced from both experimental observations and experimentally validated multi-physics finite element model simulations [63]. A 2200 mAh capacity commercial 18650 Li-ion battery was selected as the subject of experimental validation. The anode and cathode materials utilized were LixC6 and LiCoO2, respectively. The charging and cutoff voltages employed were 4.2 V and 2.5 V, respectively. The multiphysics coupling model comprises three distinct models: a 1D battery model, a short-circuit model, and a 3D thermal model. The coupling model is established through the exchange of information between different signals among the three models, as illustrated in Fig. 2.

1D battery model and short-circuit model interact with information through the voltage and current density of the cell:

$$U^{1D} = U^{St} \tag{1}$$

$$i^{1D} = B\, i^{St} \tag{2}$$

where U^{1D} and U^{St} are the voltages of the 1D model and the short-circuit model, respectively. i^{1D} and i^{St} are the current densities of the 1D model and the short-circuit model, respectively. B is the coefficient characterizing the relationship, the exact value of which can be found in [64]. 1D battery model and the 3D thermal model utilize heat production rate, loading heat rate, temperature, and average temperature for information transfer:

$$q^{1D} = q^{Tl} \tag{3}$$

$$T^{1D} = T^{Tl} \tag{4}$$

where q^{1D} and q^{Tl} are the heat production rate of the 1D battery model and the loading heat rate of the 3D thermal model, respectively. T^{1D} and T^{Tl} are the temperatures of the 1D battery model and the average temperature of the 3D thermal model, respectively [65]. It is important to highlight that the q^{1D} derived from the 1D battery model analysis is integrated into the 3D thermal model, where the calculation is performed to determine the temperature T^{Tl}. This temperature value is subsequently fed back as input into the 1D battery model. The coupling between the 1D battery model and the 3D thermal model is established through the exchange and utilization of these two variables. q^{1D} consists of four parts, reaction heat rate q^a, joule heat rate q^j, resistance heat rate from current collectors q^r, and irreversible heat rate q^i:

$$q^{1D} = q^a + q^j + q^r + q^i \tag{5}$$

The short-circuit model is then coupled to the 3D thermal model through the heat production rate and the overall heat rate:

$$q^{Ta} = q^{St} S^{St} (L^{Ng} + L^{Ps}) N^{St}(t)/2 = C\, q^{St} \tag{6}$$

where q^{Ta} and q^{St} are the overall heat rate of the 3D thermal model and the heat production rate of the short-circuit model, respectively. The coefficient C is related to the geometrical parameters of the cell. Nevertheless, given the intricate nature of the battery's structure and electrochemical processes, this study establishes thermal boundary conditions as uniform heat generation and isotropic heat transfer throughout to streamline the model. The simplified model is subsequently validated through experimentation, with simulation outcomes closely aligning with test data, thus confirming the model's validity [64].

Through the interaction of this information, a model of the battery's multiphysics field coupling is constructed, which is experimentally verified for its validity. This multi-physical field coupled model is used to generate current, voltage, and temperature datasets for batteries subjected to mechanical abuse at different SOCs. After acquiring the data, it needs to be first normalized, which is a data preprocessing technique used to unify the range of values between different features for better comparison and analysis in machine learning algorithms. Common data normalization methods include min–max normalization, Z-score normalization, decimal scaling, and range normalization, in

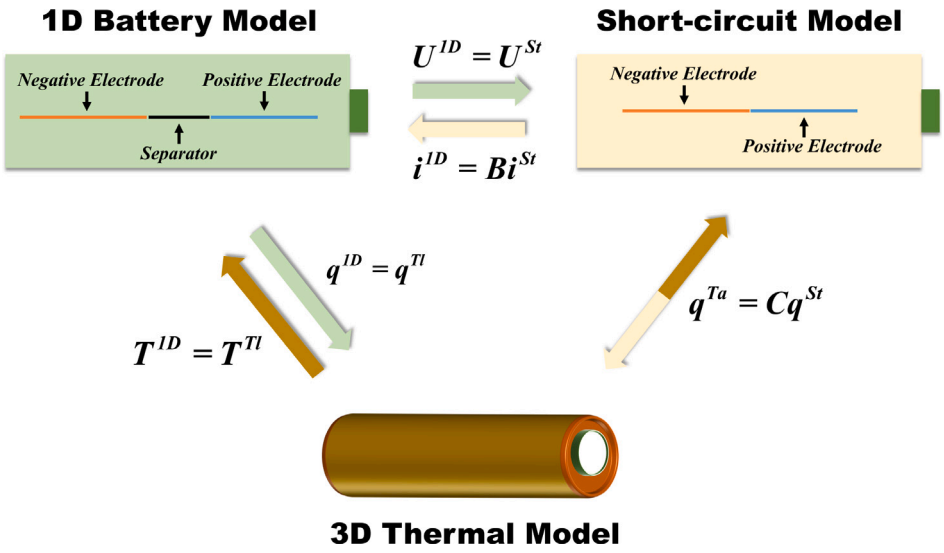

Fig. 2. Multi-physics field coupling modeling of batteries.

this work min–max normalization method is utilized which can be expressed as:

$$x_k^* = \frac{x_k - \min\left(x_k\right)}{\max\left(x_k\right) - \min\left(x_k\right)}. \tag{7}$$

where x_k and x_k^* represent the normalized and original values of the kth column, respectively, and $\min\left(x_k\right)$ and $\max\left(x_k\right)$ represent the minimum and maximum values of the kth column, respectively [66].

3. Failure mode recognition

In this section, the SOM-BP model is employed to identify failure modes. The SOM-BP model integrates the SOM model to address the limitations of the conventional BP model through the amalgamation of supervised and unsupervised learning characteristics, thereby offering notable benefits in the context of classification tasks. SOM represents a type of unsupervised neural network that diverges from conventional neural networks in its utilization of a competitive learning strategy instead of relying on backward transmission and loss function for training. In this approach, neurons compete with each other to iteratively optimize the network. A typical SOM model comprises an input layer and a competitive layer, with neuron nodes organized in a regular two-dimensional array, diverging from the structure of conventional feed-forward neural networks. Common configurations include a square grid or a square-hexagonal grid, with the latter being employed in this study. Each individual attribute of the input vector is linked to each neuron node within the competitive layer of the SOM network via specific weights. There are no direct connections between these neuron nodes; however, neighboring nodes engage in a neighborhood-like interaction during the training phase.

Initially, the weights of all neuron nodes are initialized with minute random values. Subsequently, the degree of correspondence between different neuron nodes and the input vector is determined using the Euclidean distance for each input vector:

$$\|x(t) - w_c(t)\| = min\{\|x(t) - w_i(t)\|, i \in A\} \tag{8}$$

where $x(t)$ is the input vector (displacement, force, and force increment), $w_i(t)$ is the weight of any node i in the competitive layer, and $w_c(t)$ is the weight of the winning node [67]. The neuron node exhibiting the highest degree of similarity is designated as the winning node (the best matching unit), through the application of a competition rule. Subsequently, the nodes encompassed within the winning neighborhood are identified according to the domain's radius, and the magnitude of the update for each node is computed using the neighborhood function to adjust the weight of the neuron nodes. This approach is founded on the principle that the proximity of a node to the winning node corresponds to a greater update magnitude, while the greater distance from the winning node results in a smaller update magnitude:

$$w_i(t+1) = w_i(t) + \alpha(t)h_{ci}(t)d[x(t), w_i(t)], \ \forall_i \in A \tag{9}$$

where $\alpha(t)$ is the learning rate, d is the Euclidean distance, and $h_{ci}(t)$ is the neighborhood function value between node i and the winning node c [67]. The neighborhood function is usually chosen as a Gaussian nearest neighbor function to characterize the relationship between strength and distance in the neighborhood. Following this method, the input vectors can be clustered by iterative loops.

The BP neural network also referred to as the backpropagation neural network, is a widely utilized artificial neural network model. This supervised learning algorithm is employed to facilitate the training of neural networks to execute classification and regression tasks. A BP neural network is comprised of an input layer, a hidden layer, and an output layer, with interconnections between neurons in adjacent layers. Through the utilization of the BP algorithm, the network iteratively adjusts the connection weights during training to minimize the disparity between the predicted output and the true output. The BP algorithm comprises two primary stages: forward propagation and backpropagation. During forward propagation, the input data is transmitted through the network, and the resulting output values are computed. In backpropagation, the output error is calculated and the connection weights are adjusted according to the error to minimize the error:

$$\mathbf{X^n} = (\mathbf{Z^n}) = \sigma(\mathbf{W^n}\ \mathbf{X^{n-1}} + \mathbf{B^n}) \tag{10}$$

$$\mathbf{W^n} = \mathbf{W^n} - \alpha\ \frac{\partial \mathbf{L}}{\partial \mathbf{W}} \tag{11}$$

$$\mathbf{B^n} = \mathbf{B^n} - \alpha\ \frac{\partial \mathbf{L}}{\partial \mathbf{B}} \tag{12}$$

where $\mathbf{X^n}$ and $\mathbf{B^n}$, respectively, represent the output value vector and bias matrix of neurons in the hidden or output layer, $\mathbf{W^n}$ represents the weight matrix from the competing layer neurons to the hidden layer neurons or the hidden layer neurons to the output layer neurons. α and $\mathbf{L}$ represent the learning rate and loss function, respectively [68]. The BP neural network is extensively utilized across various domains such as image recognition, speech recognition, and natural language processing due to its robust nonlinear fitting capability and adeptness in handling intricate data patterns, rendering it a prevalent choice in

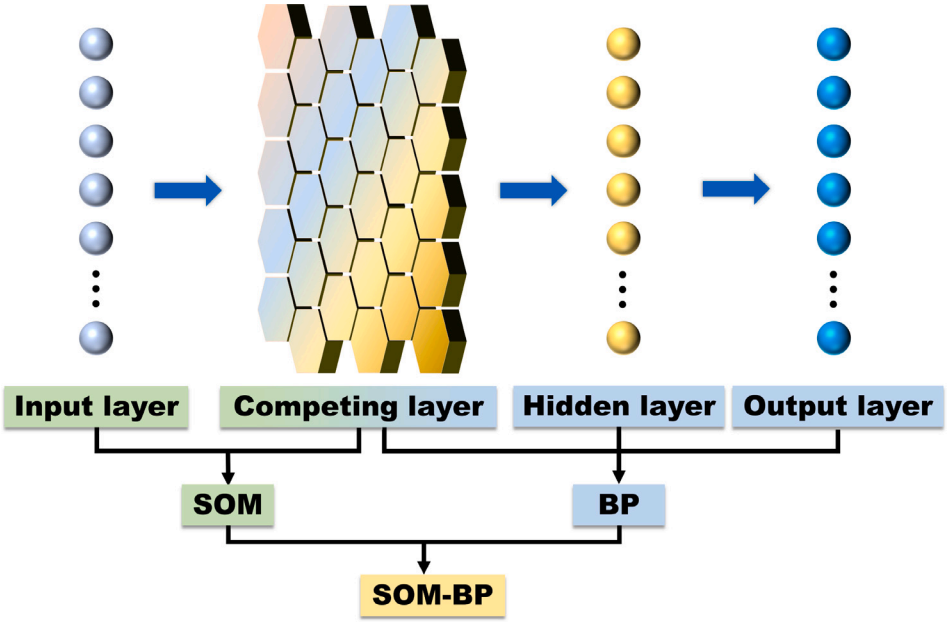

Fig. 3. Logical framework of the SOM-BP.

practical implementations. Nevertheless, BP neural networks are not without their challenges and constraints. One such issue is the substantial demand for data and computational resources during the training process, resulting in prolonged training times. Furthermore, the selection of network structure and parameters significantly influences the outcomes and necessitates the expertise of seasoned professionals for adjustments. Additionally, BP neural networks are susceptible to converging towards local optimal solutions, underscoring the importance of carefully selecting initial parameters and learning rates to mitigate this issue.

The SOM-BP model integrates the unsupervised learning function of self-organizing mapping with the supervised learning function of backpropagation. In the SOM-BP model, the input data are first clustered and downscaled using the self-organizing mapping algorithm. The subsequent low-dimensional representations are utilized as inputs for the back-propagation neural network, which employs the back-propagation algorithm to conduct supervised learning to adjust the network weights in classification or regression tasks. The integration of the SOM-BP model enables the neural network to exhibit characteristics of both unsupervised and supervised learning, enhancing its capacity to effectively process intricate data patterns and enhance the model's generalization capability. This amalgamation has demonstrated promising outcomes in various practical contexts, particularly within the domains of data mining and pattern recognition. The SOM-BP model is comprised of four distinct layers, namely the input layer, competitive layer, hidden layer, and output layer. The primary objective of this model is to leverage the competitive layer of the SOM model as the input layer of the BP model, to enhance the classification prediction capabilities of the BP model, and the underlying principle is shown in Fig. 3.

The force–displacement measurements were obtained for three different conditions: bending, compression, and indentation, with consistent sampling intervals. A total of 600 sets of data were gathered for each condition. The inputs for the SOM-BP model training included the force, displacement, and force increment for each condition, in order to identify and distinguish various failure modes. It is worth noting that these 1800 sets of data are randomly disrupted and divided into a training set and a test set according to the ratio of 70% and 30%, respectively. The training dataset is utilized for constructing the failure pattern recognition model, while the test dataset is employed for assessing the model's efficacy. The data are shown in Table 3. Fig. 4 depicts the clustering effect of the SOM model. Fig. 4a depicts the neighborhood weight distances for the SOM model, where blue hexagons indicate neurons and red lines connect neighboring neurons. The hue within the area encompassing the red line represents the proximity of neurons. A deeper shade signifies a greater distance, while a lighter shade signifies a closer distance. Fig. 4b shows the neuron locations in the topology and indicates how many observations are associated with each neuron. Fig. 5 plots the weight plane for each element of the input feature. The diagram illustrates the connections between each input and neuron, with varying shades representing the strength of the connections. If the connection patterns of two features closely resemble each other, it can be inferred that they are highly correlated. The illustration in Fig. 6 displays the classification outcomes of the SOM-BP model for both the training and test sets. In this case, the training set has a recognition correctness of 99.5% and a recognition error rate of 0.5%, and the test set has a recognition correctness of 99.4% and an error rate of 0.6%. The results indicate that the SOM-BP model demonstrates a high level of accuracy in identifying failure modes.

Table 3
Data in three failure modes.

Data label	Displacement (mm)	Force (N)	Force increment (N)	Failure mode
1	0.01	152.67	229.01	Compression
2	0.04	381.68	76.34	Compression
3	0.12	305.34	152.67	Indentation
4	0.48	152.67	152.67	Bending
5	2.10	1984.73	152.67	Indentation
6	2.11	305.34	0.00	Bending
7	2.68	4274.81	76.34	Compression
8	4.72	763.36	152.67	Bending
9	4.89	15 267.18	152.67	Compression
10	4.90	15 419.85	76.34	Compression
…	…	…	…	…
1800	5.90	10 916.03	76.34	Indentation

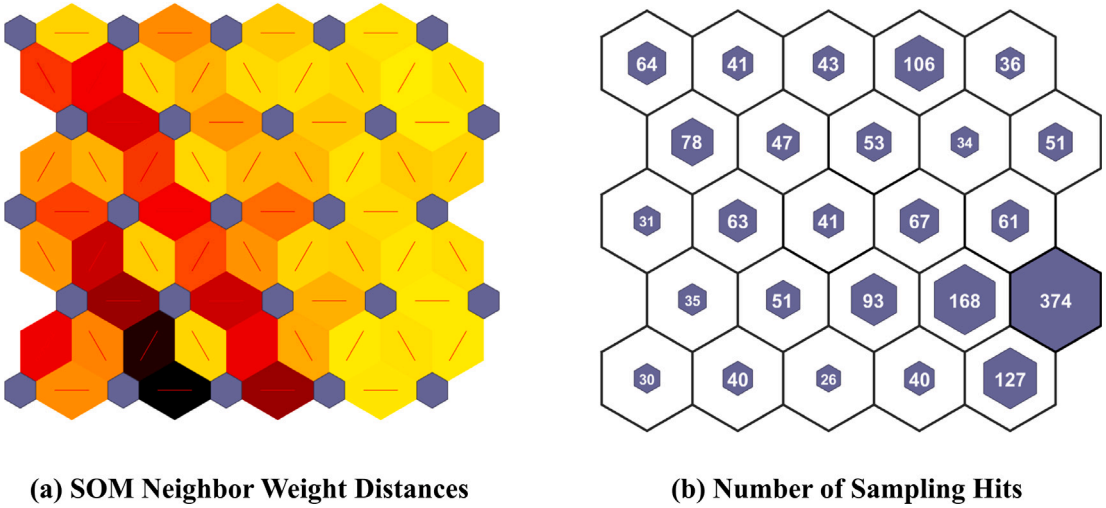

Fig. 4. Clustering results for SOM. (For interpretation of the references to color in this figure legend, the reader is referred to the web version of this article.)

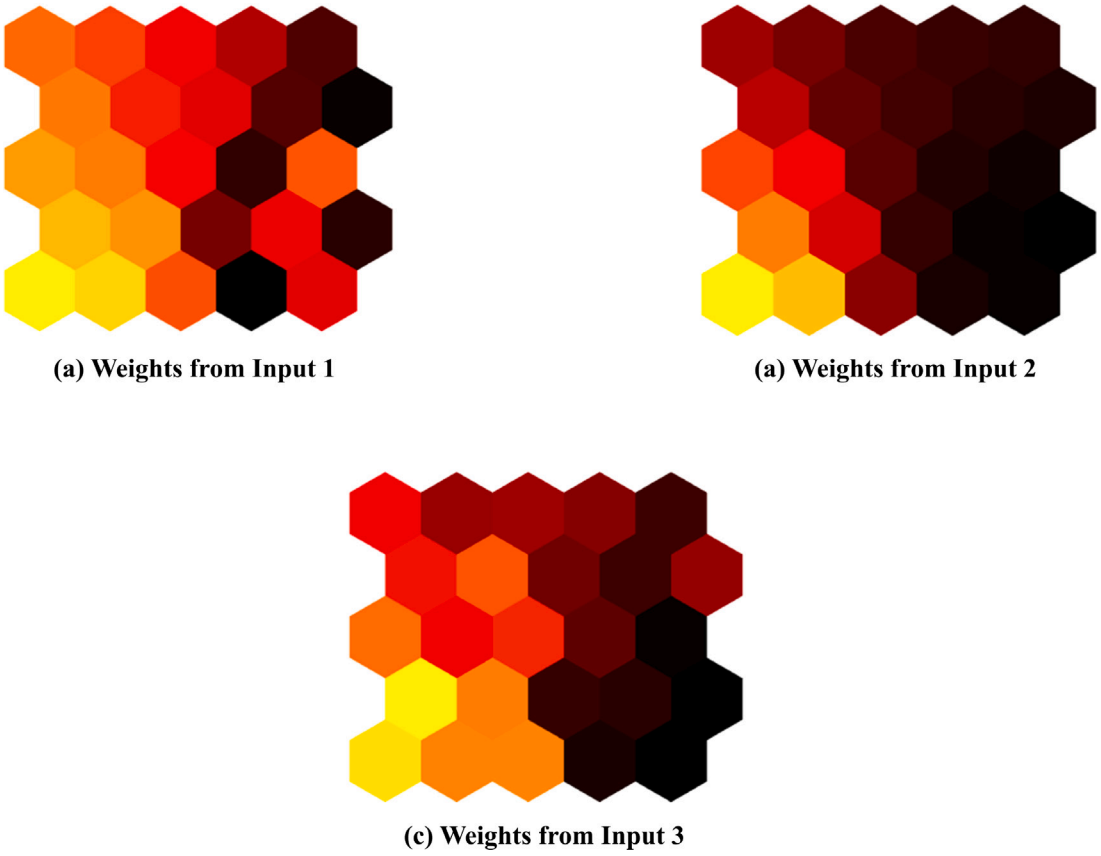

Fig. 5. The weight plane for each input.

4. Pre-short-circuit warning

In this section, the SVR-based optimization algorithm is utilized to provide an early warning of the short-circuit time before the short-circuit occurs and the time of mechanical failure, as well as a prediction of the temperature and voltage at the subsequent moment. The support vector machine (SVM) is a computational algorithm designed for binary classification tasks, and it presents distinct advantages in the domain of classification problem-solving. In addressing regression prediction challenges, SVR is introduced as an extension of the fundamental concept of SVM. The key differentiation between SVR and SVM resides in their underlying principles. While SVM is designed to discern a separating hyperplane that effectively categorizes the training dataset and maximizes the geometric margin, SVR is oriented towards minimizing the collective deviation of all data points from the hyperplane. In contrast to SVM's emphasis on identifying a separating plane for multiple classes of data points, SVR is focused on a singular class of data points and endeavors to minimize the overall deviation from the hyperplane, the principle is shown in Fig. 7.

The conventional regression approach assumes that the prediction is accurate when the regression value y_i exactly matches the true value y, and its loss is typically determined using the root mean square value

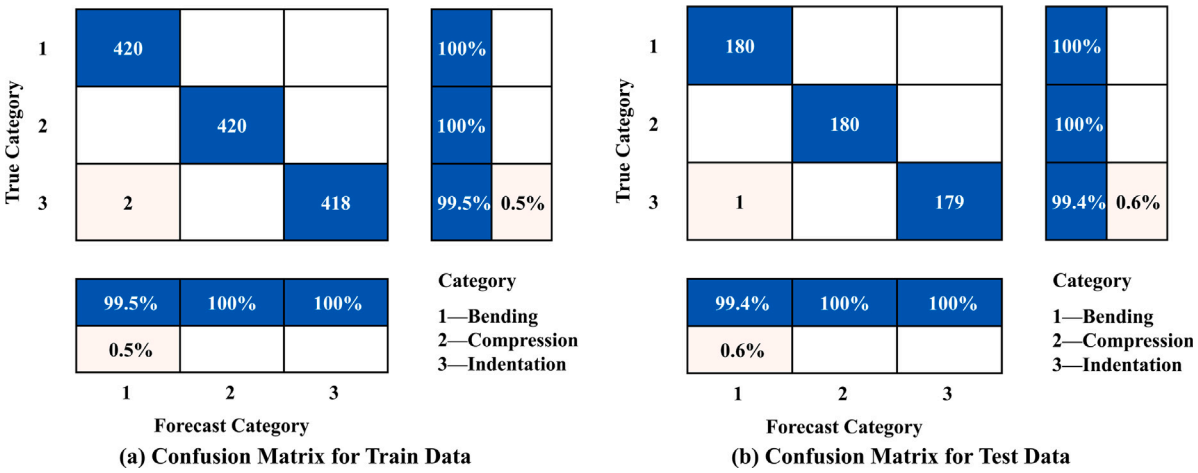

Fig. 6. Recognition accuracy of the SOM-BP model.

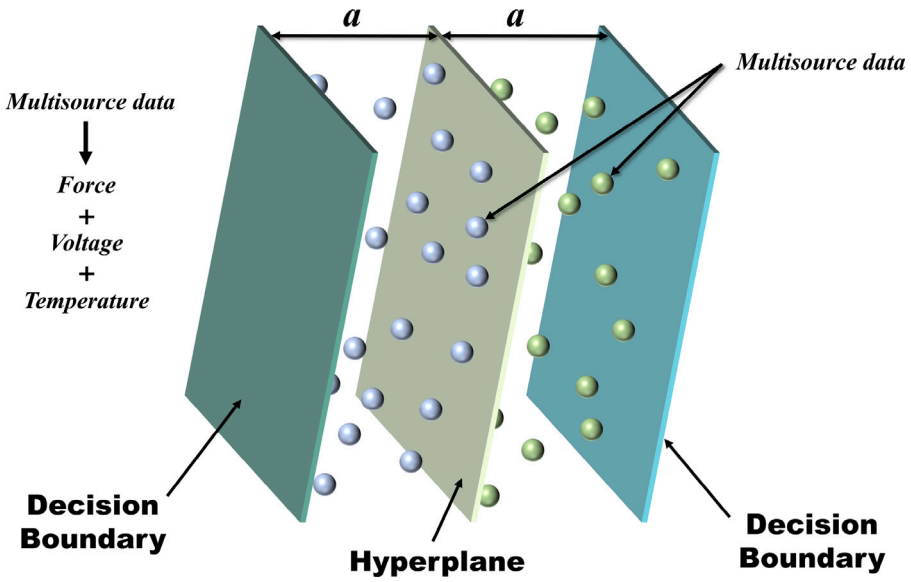

Fig. 7. Principles of the SVR model.

and other relevant methods. SVR establishes an acceptable deviation threshold (a) for the dataset, under the condition that the difference between the actual value (y) and the predicted value (y_i) falls within a specified range. When the deviation exceeds a, the model's prediction is deemed inaccurate, and the loss value for out-of-range data points is subsequently computed. A hyperplane in space can be determined by the normal vector $\mathbf{W}$ and the intercept $\mathbf{b}$ with the equation $\mathbf{X}^{\mathrm{T}}\mathbf{W}+\mathbf{b}=\mathbf{0}$. Hence, the fundamental concept of SVR may be modified to address the optimal solution of the given equation [69], aiming to minimize the distance from all sample points to the hyperplane:

$$\min \frac{1}{2}\|w\|^2 \quad \text{s.t.} \ \left|y_i - \left(x^{\mathrm{T}}w + b\right)\right| \le a \tag{13}$$

$$\|w\| = \sqrt{w_1^2 + \cdots w_n^2} \tag{14}$$

The WOA algorithm is a novel heuristic optimization approach inspired by the hunting behavior of humpback whales. In this algorithm, the position of each humpback whale corresponds to a viable solution. Humpback whales employ a unique hunting technique known as the bubble-net predation strategy in marine environments, and this behavior can be integrated into the optimization of the SVR [70,71]. Likewise, the TSO algorithm emulates the hunting patterns of tuna schools, which employ cohesive spirals and communication among individuals to track and capture their prey. This involves the transmission of information between adjacent tuna as they trail one another. According to the aforementioned principle, the spiral foraging approach utilized in SVR can enhance the predictive regression performance of SVR. Both WOA-SVR and TSO-SVR aim to identify the best solution by converting the parameter optimization issue of the SVR model into a multi-dimensional search problem and iteratively adjusting the parameters by simulating the behavior of a fish population to determine the optimal model parameters. WOA-SVR and TSO-SVR demonstrate superior efficacy in addressing intricate regression challenges, particularly when dealing with high-dimensional data and intricate nonlinear associations. Nevertheless, these algorithms emulate distinct animal behaviors and search tactics, potentially yielding varying outcomes across diverse problem domains and data attributes. Consequently, in real-world scenarios, it is imperative to carefully choose optimization algorithms based on the specific problem attributes and data characteristics to attain optimal optimization outcomes.

In this work, the two models are utilized separately to compare their accuracy. Sampling at 1s intervals, 90 sets of data were collected, and the data set was randomized and divided into training set and test set in the ratio of 80% and 20%, and the collected data are shown in Table 4. In the construction of the early warning model,

Table 4
Battery short-circuit pre-warning data.

Data label	Force (N)	Voltage (V)	Temperature (°C)	Mechanical failure time (s)	Short-circuit time (s)	Next voltage (V)	Next temperature (°C)
1	273.9	3.580	18.447	27	58	3.564	18.447
2	219.5	3.580	18.447	46	77	3.580	18.447
3	9.3	3.580	18.835	89	120	3.580	18.835
4	105.8	3.580	18.835	67	98	3.580	18.835
5	65.4	3.580	18.835	75	106	3.580	18.835
6	40.5	3.580	18.835	81	112	3.580	18.835
7	266.1	3.580	18.447	32	63	3.580	18.447
8	239.7	3.580	18.447	41	72	3.580	18.447
9	56.0	3.580	18.835	77	108	3.580	18.835
10	245.9	3.580	18.447	39	70	3.580	18.447
…	…	…	…	…	…	…	…
90	213.2	3.580	18.447	47	78	3.580	18.447

Table 5
Accuracy of WOA-SVR prediction model.

Parameters	R^2	MAE	MAPE	RMSE	ME
Mechanical failure time remaining (s)	0.99961	0.43650	0.03819	0.55170	1.38640
Short-circuit time remaining (s)	0.99958	0.46816	0.00759	0.59664	1.12450
Next voltage (V)	0.99932	0.00014	0.00004	0.00017	0.00043
Next temperature (°C)	0.99904	0.00695	0.00037	0.00966	0.02363

the model takes into account the force, voltage, and temperature as its input parameters. The model then generates outputs in the form of the remaining time until mechanical failure, the remaining time until short-circuit occurs, and the anticipated voltage and temperature at the subsequent moment. Hence, by employing this framework, the cloud has the capability to anticipate the remaining time to mechanical failure and short-circuiting when it detects anomalous data from the vehicle's battery. Simultaneously, it can also acquire the voltage and temperature for the subsequent moment, thereby offering timely alerts to occupants and safeguarding passengers' safety.

The accuracy of the constructed WOA-SVR model and TSO-SVR and their comparative plots are shown in Figs. 8 and 9. The precision plot consists of a combination of two graphs, the box plot and the scatter plot. The box plot contains the elements perc(25,75), 1.5 Scope within IQR, Median, and Mean, and the mean value of the model is also labeled on the plot, with the small ball on the right side as the specific distribution of the values. The curves represent the distribution of the data in a normal manner. The analysis of the different components of the box plot indicates the conformity of the predictive model with the reference value, thereby indicating the high precision of the WOA-SVR and TSO-SVR models in forecasting the time remaining until mechanical failure and short-circuit failure. In the scatter plot, the black and red spheres symbolize the distribution of the predicted and reference values, respectively. The close alignment of the centers of the black and red spheres in the plot demonstrates the high accuracy of the WOA-SVR and TSO-SVR models in forecasting voltage and temperature for the subsequent time.

Table 5 lists the specific accuracies of the WOA-SVR prediction model, whose evaluation parameters consist of coefficient of determination (R^2), mean absolute error (MAE), mean absolute percentage error (MAPE), root mean square value (RMSE) & maximum absolute error (ME), and similarly, Table 6 lists the specific accuracies of the TSO-SVR prediction model. The comparative analysis reveals that the WOA-SVR model demonstrates a slight edge in predicting battery mechanical failure time and short circuit time warnings, whereas the TSO-SVR model excels in forecasting voltage and temperature for the subsequent moment. It is noteworthy that both models exhibit relatively high accuracy in their predictions. The model can be hosted in the cloud, where it does not have to interact with real-time data from the vehicle. The cloud can continuously monitor the mechanical status of the battery, including temperature and voltage, to give advance notice of potential mechanical issues or battery short-circuits in the vehicle.

5. Post-short-circuit prediction

In this section, the RF algorithm is presented for creating a model to predict post-short-circuit outcomes, and its precision is evaluated against the WOA-SVR and TOA-SVR models. The RF algorithm is an integrated learning method that makes predictions by constructing multiple decision trees [72]. The fundamental concept behind the RF algorithm involves creating several decision trees by randomly choosing a portion of the dataset and a portion of the features. These decision trees' predictions are then combined to produce more reliable and precise results, as illustrated in Fig. 10. The RF algorithm constructs decision trees by randomly selecting subsets of data and features, thus reducing the risk of overfitting. Predictions from multiple decision trees are combined using integrated learning, resulting in more stable and accurate predictions. The concept of integrated learning involves training several weak models to be combined into a powerful model that outperforms a single weak model. The RF algorithm is capable of processing large datasets, it has fast prediction speed, and excels in both classification and regression tasks, making it widely utilized in real-world scenarios. It can be applied to diverse datasets and typically delivers superior prediction outcomes.

To develop an RF prediction model, the initial step involves the creation of a decision tree, each of which is built by training a random subset of the dataset. This element of randomness serves to mitigate the potential for overfitting. Subsequently, during the construction of each decision tree, RF employs a random selection of features, resulting in the training of each decision tree based on a distinct subset of features. This approach serves to enhance the diversity of the model. Ultimately, when a prediction is required, RF amalgamates the predictions from each decision tree, typically utilizing voting or averaging to derive the final prediction. When solving regression prediction problems, there are usually two algorithms to summarize the prediction results of different decision trees, the first one is the simple averaging method which can be described as:

$$F_T(x) = \frac{1}{T}\sum_{t=1}^{T} D_t(x) \tag{15}$$

where $F_T(x)$ is the output of the random forest algorithm (temperature, next current, next voltage), T is the number of decision trees, and $D_t(x)$ is the output of the tth decision tree [72]. The second is the weighted average method which can be described as:

$$F_T(x) = \sum_{t=1}^{T} \omega_t D_t(x) \tag{16}$$

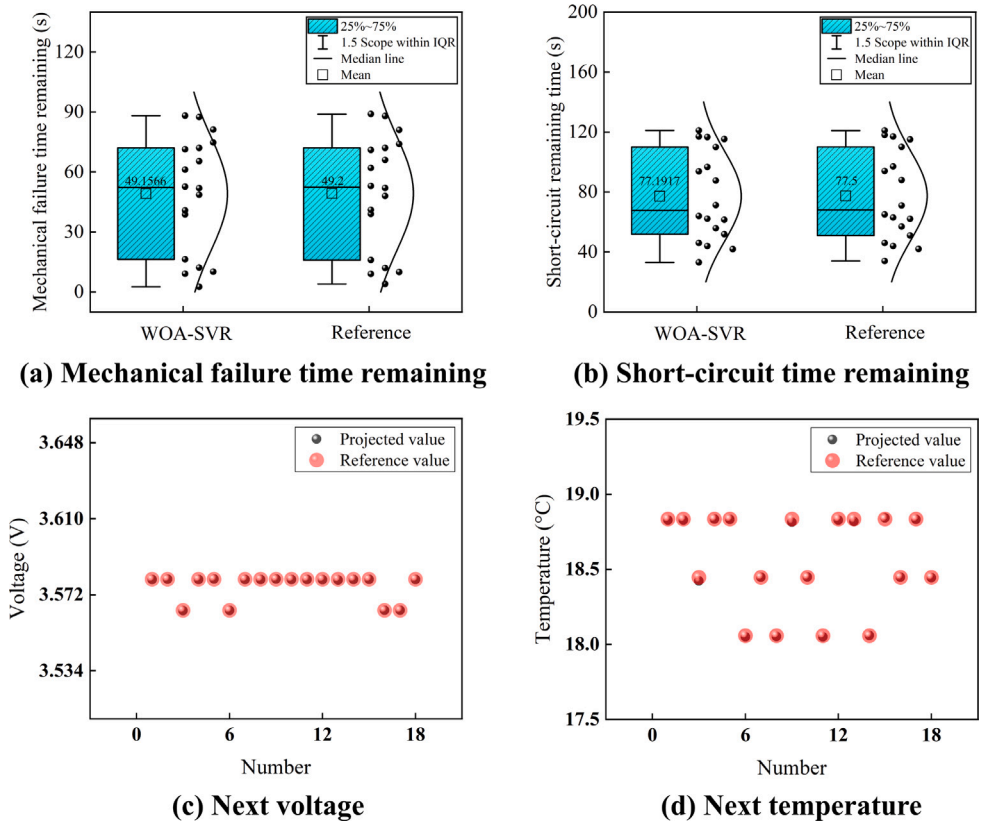

Fig. 8. Accuracy of WOA-SVR prediction model.

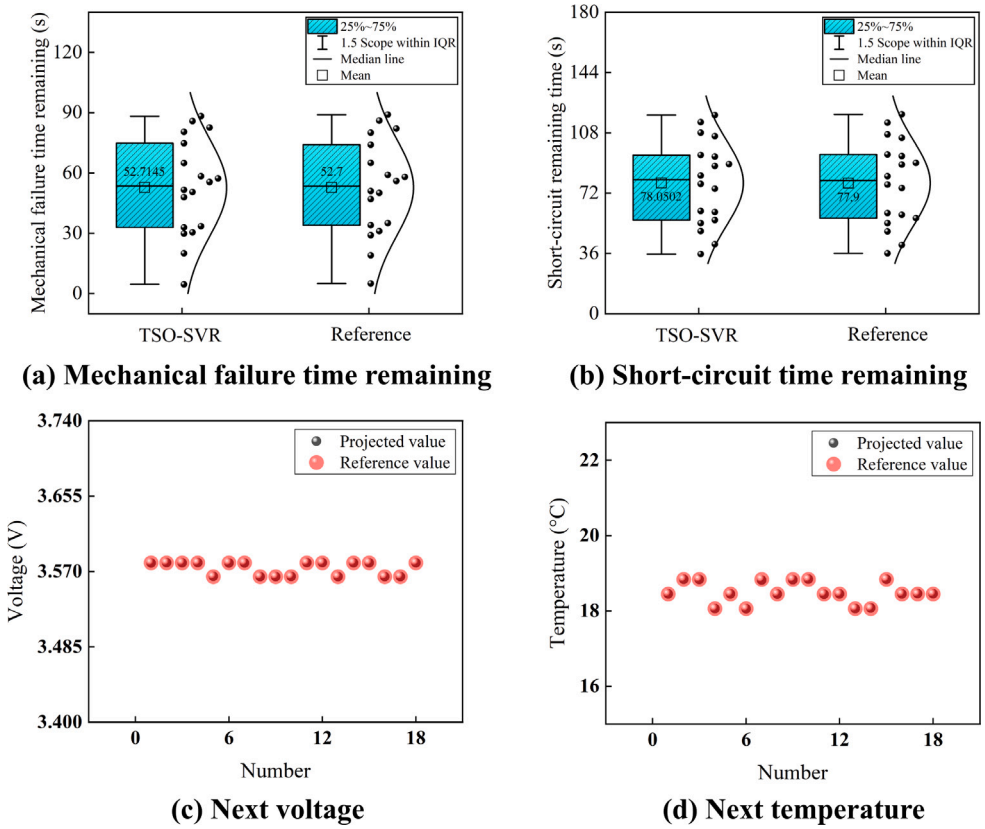

Fig. 9. Accuracy of TSO-SVR prediction model.

Table 6
Accuracy of TSO-SVR prediction model.

Parameters	R^2	MAE	MAPE	RMSE	ME
Mechanical failure time remaining (s)	0.99899	0.67353	0.02093	0.74285	1.50670
Short-circuit time remaining (s)	0.99906	0.63689	0.00903	0.75911	1.64230
Next voltage (V)	0.99964	0.00012	0.00003	0.00014	0.00036
Next temperature (°C)	0.99934	0.00504	0.00027	0.00733	0.01899

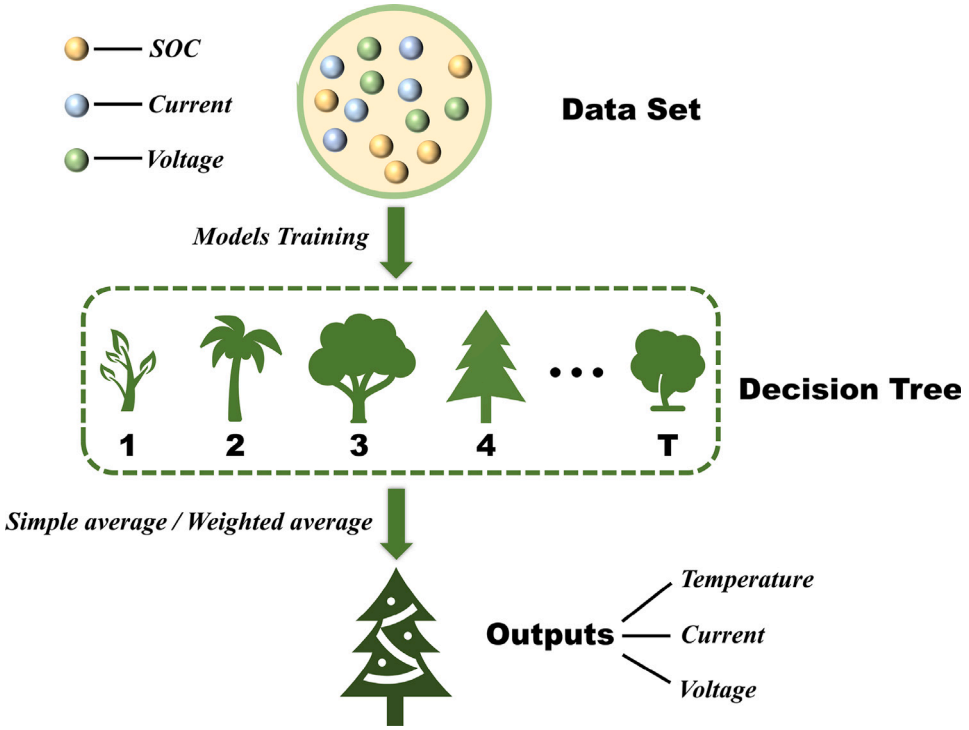

Fig. 10. Principles of the RF model.

where ω_t is the weight of different decision trees, the smaller the error rate the larger the weight of the decision tree, it is worth noting that $\sum_{t=1}^{T} \omega_t = 1$ [73].

The RF algorithm demonstrates effectiveness in managing extensive datasets and exhibits high efficiency in both training and prediction processes. Additionally, it displays resilience in handling missing values and noisy data and is capable of addressing complex data scenarios. However, due to the inclusion of parameters such as the number of decision trees, the maximum depth of each tree, and the feature selection strategy, the algorithm requires tuning through cross-validation and other techniques. RF is extensively utilized in practical scenarios, particularly for handling high-dimensional and complex data, and it often yields superior predictive outcomes. Owing to its integrated learning attributes, RF can effectively mitigate the risk of overfitting and exhibits enhanced generalization capabilities in comparison to a standalone decision tree. Likewise, the data for current, voltage, and temperature at various SOCs were collected under uniform mechanical stress conditions, with a sampling frequency of 1 s. It is noteworthy that 301 sets of data were acquired at SOCs of 0, 0.3, 0.5, 0.7, and 1.0, respectively, as shown in Table 7. The dataset comprising 1505 sets of data is partitioned into training and test sets at an 80% to 20% ratio. These data are employed to construct prediction models, namely WOA-SVR, TSO-SVR, and RF, with inputs including SOC, current, and voltage. These models can be applied to forecast temperature, as well as predict current and voltage for the subsequent moment. The accuracy of the constructed WOA-SVR model, TSO-SVR model, RF model, and their comparative violin plots are shown in Figs. 11, 12 and 13.

The predictive accuracy of each predictive model is compared here using violin plots, where the inside of the violin is part of the elements of the box plot, such as perc(25,75), 1.5 Scope within IQR, and Median, and its outside violin shape characterizes the distribution of the data. To measure the prediction accuracy of these three models more clearly, the error functions R^2, MAE, MAPE, RMSE, and ME were used to quantify the accuracy of the three prediction models. The accuracies of the WOA-SVR, TSO-SVR, and RF models are shown in Tables 8, 9, and 10, respectively. The comparison indicates that the TSO-SVR model demonstrates superior accuracy in forecasting temperature and voltage, whereas the RF model exhibits higher precision in predicting current, potentially due to its internal mechanism, which involves the collective impact of multiple decision trees.

Further, the fitted surface plot of SOC versus voltage, current, and temperature is shown in Fig. 14. The results demonstrate the high risk of temperature rise and thermal runaway at high SOC, and the need for more safety measures to avoid fires at high SOC to protect the lives of passengers. Moreover, the computational costs associated with the SOM-BP, WOA-SVR, TSO-SVR, and RF models are tabulated, with the SOM-BP model requiring an identification time of 4.384 s, and the WOA-SVR, TSO-SVR, and RF models necessitating computational times of 2.998 s, 4.869 s, and 1.230 s, respectively. It is critical to note that the computational time of a model is influenced by the computational power of the device being used. Leveraging the robust computational capabilities of a high-performance computing platform, such as a cloud infrastructure, can significantly reduce computation time, thereby enabling real-time information exchange between the vehicle and the cloud.

This work utilizes the mechanical, electrical, and thermal signals of a battery undergoing mechanical abuse to provide a predictive early warning scheme for battery safety in collaboration with cloud

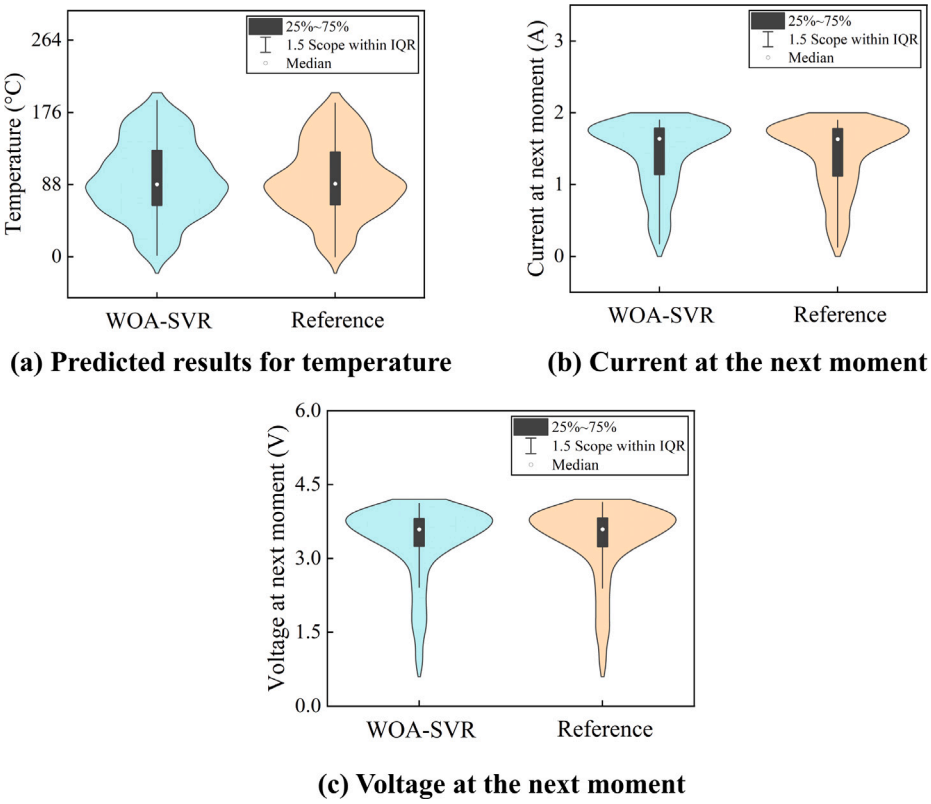

Fig. 11. Accuracy of WOA-SVR prediction model.

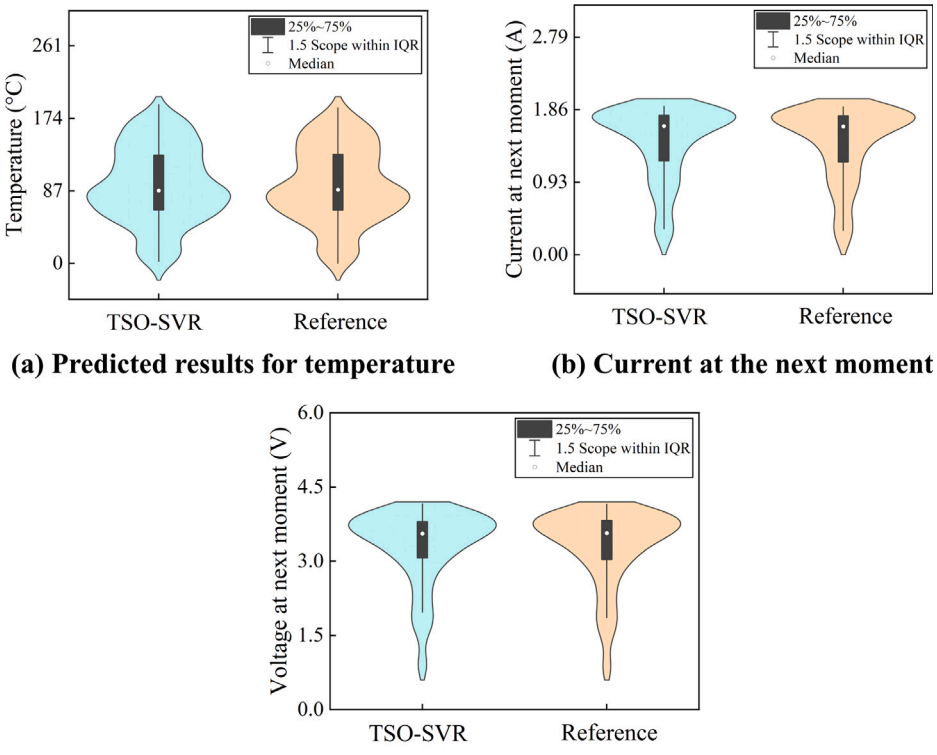

Fig. 12. Accuracy of TSO-SVR prediction model.

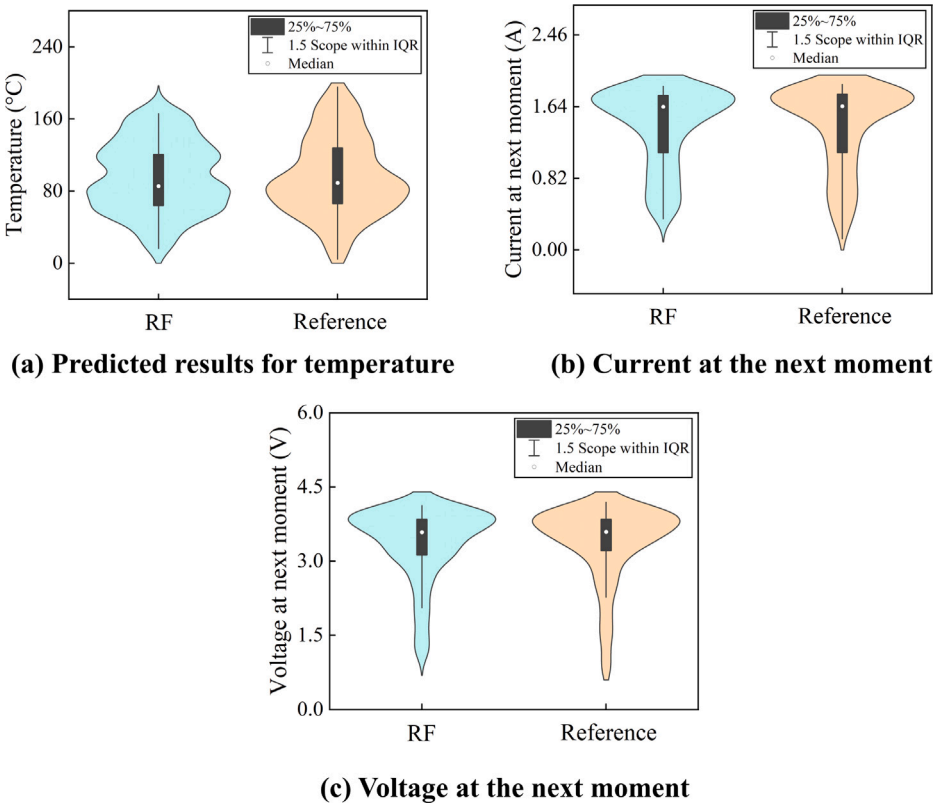

Fig. 13. Accuracy of RF prediction model.

Table 7
Data after battery short-circuit.

Data label	SOC	Current (A)	Voltage (V)	Temperature (°C)	Next current (A)	Next voltage (V)
1	0	0.126	3.465	0.000	0.126	3.465
2	0.7	1.782	3.822	107.759	1.782	3.822
3	0.5	1.644	3.516	149.425	1.644	3.516
4	0.3	1.075	2.293	86.207	1.069	2.280
5	1	1.218	4.102	53.161	1.391	4.102
6	1	1.885	4.025	117.816	1.885	4.025
7	0	1.011	3.389	37.356	1.011	3.389
8	0.7	1.770	3.796	170.977	1.770	3.796
9	1	1.862	3.975	173.851	1.862	3.975
10	0.5	1.701	3.618	76.149	1.701	3.618
…	…	…	…	…	…	…
1505	0.5	1.667	3.567	112.069	1.667	3.567

Table 8
Accuracy of WOA-SVR prediction model.

Parameters	R^2	MAE	MAPE	RMSE	ME
Temperature (°C)	0.97799	3.86970	0.07896	6.62560	62.45730
Next current (A)	0.95555	0.01741	0.01785	0.10211	1.59130
Next voltage (V)	0.99794	0.02324	0.00858	0.03376	0.32895

Table 9
Accuracy of TSO-SVR prediction model.

Parameters	R^2	MAE	MAPE	RMSE	ME
Temperature (°C)	0.98874	3.19340	0.05079	4.81210	23.10290
Next current (A)	0.95987	0.01655	0.01708	0.09426	1.59350
Next voltage (V)	0.99846	0.02297	0.00878	0.03004	0.16560

Table 10
Accuracy of RF prediction model.

Parameters	R^2	MAE	MAPE	RMSE	ME
Temperature (°C)	0.97799	3.86970	0.07896	6.62560	62.45730
Next current (A)	0.95555	0.01741	0.01785	0.10211	1.59130
Next voltage (V)	0.99794	0.02324	0.00858	0.03376	0.32895

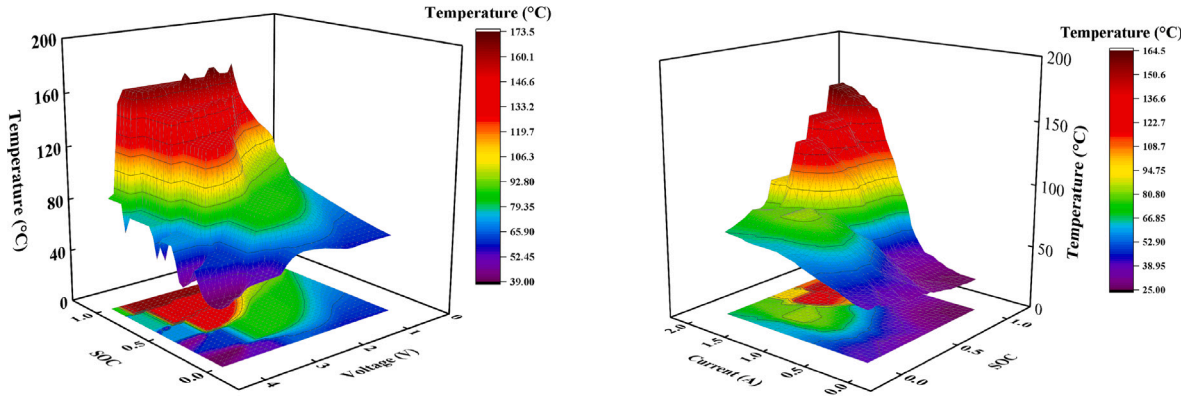

(a) SOC, Voltage vs. Temperature **(b) SOC, Current vs. Temperature**

Fig. 14. Relationship between SOC, Voltage, Current and Temperature.

technology. It contributes mainly from three perspectives: failure mode recognition, pre-short-circuit warning, and post-short-circuit prediction. Upon detecting battery abuse at the vehicle level, the cloud model can be employed to forecast the time of mechanical failure and short-circuit occurrence, as well as the subsequent temperature, current, and voltage levels. This approach aims to ensure the safety of drivers and passengers, while early warnings afford occupants ample time to evacuate. However, owing to the restricted data availability, this study exclusively examines and forecasts the multivariate signal data within specific operational parameters and SOC. In the future, the collection of multivariate signals across diverse operational conditions is necessary to enhance the model's adaptability to a wide range of scenarios, enabling comprehensive prediction and early warning capabilities. Furthermore, the advancement of more sophisticated algorithms and expansive models holds the potential for precise battery prediction and warning systems. However, optimizing the balance between data volume and model complexity to enhance computational efficiency remains a key area for future development.

6. Conclusions

In this work, a cloud-based battery mechanical failure mode recognition and early warning model framework was built, which utilizes multi-source signals to predict battery failure as early as possible, thus protecting the lives of drivers and passengers. The main conclusions of this work can be summarized as follows:

(1) A model for recognizing failure modes was developed by integrating the characteristics of the unsupervised learning clustering model SOM with the supervised learning model BP. This combined model effectively identifies failure modes using mechanical signals. Specifically, the model successfully distinguishes between three modes – bending, compression, and indentation – based on battery forces, displacements, and force increments.

(2) A battery short-circuit prediction and warning model was constructed to predict the time remaining to mechanical failure and the time remaining to short-circuit of the battery, as well as the voltage and temperature at the subsequent moment. Two prediction models, WOA-SVR and TSO-SVR, were created and evaluated for accuracy. The findings indicate a remarkably high level of precision in the predictions.

(3) A predictive model for battery short-circuit events was developed to accurately forecast the variations in temperature, current, and voltage for different SOCs following short-circuit. Here, three prediction models, WOA-SVR, TSO-SVR & RF, are constructed to perform post-short-circuit prediction, and each model demonstrates different features.

This method enables the deployment of models in cloud-based systems, facilitating the generation of predictive alerts through the integration of data from the cloud and the vehicle. This is aimed at safeguarding occupants in the event of battery mechanical abuse. In the future, there will be a requirement to gather and leverage a wider range of mechanical, electrical, and thermal data to develop more precise and comprehensive prediction and warning models, thereby enhancing passengers' safety.

CRediT authorship contribution statement

Xiaoxi Zhang: Writing – original draft, Visualization, Software, Methodology, Formal analysis, Data curation, Conceptualization, Investigation, Validation. **Yongjun Pan:** Writing – review & editing, Validation, Supervision, Conceptualization. **Yangzheng Cao:** Data curation, Formal analysis, Software. **Binghe Liu:** Writing – review & editing, Funding acquisition. **Xinxin Yu:** Writing – review & editing, Validation.

Declaration of competing interest

We declare that we do not have any commercial or associative interest that represents a conflict of interest in connection with the work submitted.

Data availability

I have shared the link to my data.

Acknowledgments

This work was supported by the National Natural Science Foundation of China (Project No. 12272072).

Replication of results

The datasets analyzed during the current study can be downloaded from the figshare repository, and are available from the authors upon reasonable request, https://doi.org/10.6084/m9.figshare.24964686.

References

[1] P.V. Chombo, Y. Laoonual, A review of safety strategies of a li-ion battery, J. Power Sources 478 (2020) 228649.
[2] L. Yao, Z. Fang, Y. Xiao, J. Hou, Z. Fu, An intelligent fault diagnosis method for lithium battery systems based on grid search support vector machine, Energy 214 (2021) 118866.
[3] J. Shi, A. Rivera, D. Wu, Battery health management using physics-informed machine learning: Online degradation modeling and remaining useful life prediction, Mech. Syst. Signal Process. 179 (2022) 109347.
[4] M. Ebrahimi, M. Shafie-khah, H. Laaksonen, Uncertainty-observed virtual battery model for an electric vehicle parking lot enabling charger-sharing modelling, J. Energy Storage 89 (2024) 111578.
[5] L. Luo, S.S. Abdulkareem, A. Rezvani, M.R. Miveh, S. Samad, N. Aljojo, M. Pazhoohesh, Optimal scheduling of a renewable based microgrid considering photovoltaic system and battery energy storage under uncertainty, J. Energy Storage 28 (2020) 101306.
[6] H. Li, J. Gu, D. Zhou, Z. Cui, P. Li, C. Zhang, Rate-dependent damage and failure behavior of lithium-ion battery electrodes, Eng. Fract. Mech. (2024) 110143.
[7] W. Li, N. Wang, A. Garg, L. Gao, Multi-objective optimization of an air cooling battery thermal management system considering battery degradation and parasitic power loss, J. Energy Storage 58 (2023) 106382.
[8] B. Xu, J. Lee, D. Kwon, L. Kong, M. Pecht, Mitigation strategies for li-ion battery thermal runaway: A review, Renew. Sustain. Energy Rev. 150 (2021) 111437.
[9] A.M. Bates, Y. Preger, L. Torres-Castro, K.L. Harrison, S.J. Harris, J. Hewson, Are solid-state batteries safer than lithium-ion batteries? Joule 6 (4) (2022) 742–755.
[10] B. Liu, Y. Jia, C. Yuan, L. Wang, X. Gao, S. Yin, J. Xu, Safety issues and mechanisms of lithium-ion battery cell upon mechanical abusive loading: A review, Energy Storage Mater. 24 (2020) 85–112.
[11] Y. Pan, Y. Xiong, L. Wu, K. Diao, W. Guo, Lightweight design of an automotive battery-pack enclosure via advanced high-strength steels and size optimization, Int. J. Automot. Technol. 22 (2021) 1279–1290.
[12] L. Zhang, X. Li, M. Yang, W. Chen, High-safety separators for lithium-ion batteries and sodium-ion batteries: advances and perspective, Energy Storage Mater. 41 (2021) 522–545.
[13] Y. Zhang, R. Xiong, H. He, M.G. Pecht, Long short-term memory recurrent neural network for remaining useful life prediction of lithium-ion batteries, IEEE Trans. Veh. Technol. 67 (7) (2018) 5695–5705.
[14] Y. Pan, Y. Xiong, W. Dai, K. Diao, L. Wu, J. Wang, Crush and crash analysis of an automotive battery-pack enclosure for lightweight design, Int. J. Crashworthiness 27 (2) (2022) 500–509.
[15] Q. Xia, Y. Ren, Z. Wang, D. Yang, P. Yan, Z. Wu, B. Sun, Q. Feng, C. Qian, Safety risk assessment method for thermal abuse of lithium-ion battery pack based on multiphysics simulation and improved bisection method, Energy 264 (2023) 126228.
[16] A. Bolurian, H. Akbari, S. Mousavi, Day-ahead optimal scheduling of microgrid with considering demand side management under uncertainty, Electr. Power Syst. Res. 209 (2022) 107965.
[17] Y.-R. Lee, H.-J. Kim, M.-K. Kim, Optimal operation scheduling considering cycle aging of battery energy storage systems on stochastic unit commitments in microgrids, Energies 14 (2) (2021) 470.
[18] L. Wang, S. Chen, L. Luo, Y. Cao, Analysis of low-carbon comprehensive energy system scheduling considering multiple uncertainties, Clean Technol. Environ. Policy (2024) 1–17.
[19] M. Li, M. Aksoy, S. Samad, Optimal energy management and scheduling of a microgrid with integrated electric vehicles and cost minimization, Soft Comput. 28 (3) (2024) 2015–2034.
[20] K. Hu, B. Wang, Y. Feng, S. Cao, L. Wang, W. Li, Robust optimal scheduling of integrated energy systems considering multiple uncertainties, Energy Sci. Eng. 11 (10) (2023) 3413–3433.
[21] J. Tang, J. Liu, T. Sun, H. Kang, X. Hao, Multi-time-scale optimal scheduling of integrated energy system considering demand response, IEEE Access 11 (2023) 135891–135904.
[22] H. Chen, L. Gao, Z. Zhang, Multi-objective optimal scheduling of a microgrid with uncertainties of renewable power generation considering user satisfaction, Int. J. Electr. Power Energy Syst. 131 (2021) 107142.
[23] J. Zhao, L. Chen, Y. Wang, Q. Liu, A review of system modeling, assessment and operational optimization for integrated energy systems, Sci. China Inf. Sci. 64 (9) (2021) 191201.
[24] H. Li, X. Li, S. Chen, S. Li, Y. Kang, X. Ma, Low-carbon optimal scheduling of integrated energy system considering multiple uncertainties and electricity–heat integrated demand response, Energies 17 (1) (2024) 245.
[25] Z. Zhang, P. Wang, P. Jiang, Z. Liu, L. Fu, Energy management of ultra-short-term optimal scheduling of integrated energy system considering the characteristics of heating network, Energy 240 (2022) 122790.
[26] F. Hong, W. Cuiying, L. Lu, L. Xuan, Review of uncertainty modeling for optimal operation of integrated energy system. Front, Energy Res. 9 (2022) 641337.
[27] F.N. Budiman, M.A. Ramli, H.R. Bouchekara, A.H. Milyani, Optimal scheduling of a microgrid with power quality constraints based on demand side management under grid-connected and islanding operations, Int. J. Electr. Power Energy Syst. 155 (2024) 109650.
[28] Y. Li, B. Wang, Z. Yang, J. Li, G. Li, Optimal scheduling of integrated demand response-enabled community-integrated energy systems in uncertain environments, IEEE Trans. Ind. Appl. 58 (2) (2021) 2640–2651.
[29] H. Kim, M. Kim, J. Lee, A two-stage stochastic p-robust optimal energy trading management in microgrid operation considering uncertainty with hybrid demand response, Int. J. Electr. Power Energy Syst. 124 (2021) 106422.
[30] P. Li, Z. Wang, J. Wang, W. Yang, T. Guo, Y. Yin, Two-stage optimal operation of integrated energy system considering multiple uncertainties and integrated demand response, Energy 225 (2021) 120256.
[31] L. Wang, H. Dong, J. Lin, M. Zeng, Multi-objective optimal scheduling model with IGDT method of integrated energy system considering ladder-type carbon trading mechanism, Int. J. Electr. Power Energy Syst. 143 (2022) 108386.
[32] R. Machlev, N. Zargari, N. Chowdhury, J. Belikov, Y. Levron, A review of optimal control methods for energy storage systems-energy trading, energy balancing and electric vehicles, J. Energy Storage 32 (2020) 101787.
[33] Y. Cao, H. Wang, B. Liu, J. Xu, Modeling, validation, and analysis of swelling behaviors of lithium-ion batteries, J. Energy Storage 74 (2023) 109499.
[34] Z. Yan, Y. Zhang, J. Yu, B. Ran, Life cycle improvement of serially connected batteries system by redundancy based on failure distribution analysis, J. Energy Storage 46 (2022) 103851.
[35] J. Shin, W. Kim, K. Yoo, H. Kim, M. Han, Vehicular level battery modeling and its application to battery electric vehicle simulation, J. Power Sources 556 (2023) 232531.
[36] C. Yang, S. Xin, L. Mai, Y. You, Materials design for high-safety sodium-ion battery, Adv. Energy Mater. 11 (2) (2021) 2000974.
[37] L. Zhang, T. Gao, G. Cai, K.L. Hai, Research on electric vehicle charging safety warning model based on back propagation neural network optimized by improved gray wolf algorithm, J. Energy Storage 49 (2022) 104092.
[38] Y. Xia, Z. Shi, Q. Zhou, W. Ao, Numerical investigation on polyurea coated aluminum plate subjected to low velocity impact, Int. J. Impact Eng. 177 (2023) 104516.
[39] P. Chen, Y. Xia, Q. Zhou, S. Liu, Staggered layout of battery cells for mitigating damage in side pole collisions of electric vehicles, eTransportation 16 (2023) 100238.
[40] X. Zhang, Y. Xiong, Y. Pan, D. Xu, I. Kawsar, B. Liu, L. Hou, Deep-learning-based inverse structural design of a battery-pack system, Reliab. Eng. Syst. Saf. (2023) 109464.
[41] X. Zhang, Y. Xiong, Y. Pan, H. Du, B. Liu, Crushing stress and vibration fatigue-life optimization of a battery-pack system, Struct. Multidiscip. Optim. 66 (3) (2023) 48.
[42] S. Kohtz, Y. Xu, Z. Zheng, P. Wang, Physics-informed machine learning model for battery state of health prognostics using partial charging segments, Mech. Syst. Signal Process. 172 (2022) 109002.
[43] Q. Wang, Z. Wang, L. Zhang, P. Liu, L. Zhou, A battery capacity estimation framework combining hybrid deep neural network and regional capacity calculation based on real-world operating data, IEEE Trans. Ind. Electron. 70 (8) (2022) 8499–8508.
[44] Q. Zhang, X. Li, C. Zhou, Y. Zou, Z. Du, M. Sun, Y. Ouyang, D. Yang, Q. Liao, State-of-health estimation of batteries in an energy storage system based on the actual operating parameters, J. Power Sources 506 (2021) 230162.
[45] R. Xiong, Y. Pan, W. Shen, H. Li, F. Sun, Lithium-ion battery aging mechanisms and diagnosis method for automotive applications: Recent advances and perspectives, Renew. Sustain. Energy Rev. 131 (2020) 110048.
[46] G. Lee, D. Kwon, C. Lee, A convolutional neural network model for SOH estimation of Li-ion batteries with physical interpretability, Mech. Syst. Signal Process. 188 (2023) 110004.
[47] J. Wen, Q. Zou, C. Chen, Y. Wei, Linear correlation between state-of-health and incremental state-of-charge in Li-ion batteries and its application to SoH evaluation, Electrochim. Acta 434 (2022) 141300.
[48] X. Li, C. Yuan, X. Li, Z. Wang, State of health estimation for Li-Ion battery using incremental capacity analysis and Gaussian process regression, Energy 190 (2020) 116467.
[49] R. Xiong, F. Sun, Z. Chen, H. He, A data-driven multi-scale extended Kalman filtering based parameter and state estimation approach of lithium-ion polymer battery in electric vehicles, Appl. Energy 113 (2014) 463–476.
[50] Y. Zhang, M. Zhao, Cloud-based in-situ battery life prediction and classification using machine learning, Energy Storage Mater. (2023).
[51] P. Ying, C. Wang, Y. Xia, Role of the temperature and aging in mechanical modeling of the active coating in li-ion battery, eTransportation 18 (2023) 100273.
[52] S.-W. Park, S.-Y. Son, Techno-economic analysis for the electric vehicle battery aging management of charge point operator, Energy (2023) 128095.
[53] S. Barcellona, S. Colnago, G. Dotelli, S. Latorrata, L. Piegari, Aging effect on the variation of li-ion battery resistance as function of temperature and state of charge, J. Energy Storage 50 (2022) 104658.
[54] A.H. Ali, M.G. Yaseen, M. Aljanabi, S.A. Abed, Transfer learning: A new promising techniques, Mesop. J. Big Data 2023 (2023) 29–30.
[55] A.H. Ali, R. Thakkar, Climate changes through data science: Understanding and mitigating environmental crisis, Mesop. J. Big Data 2023 (2023) 125–137.
[56] Y. Liu, Y. Mao, H. Wang, Y. Pan, B. Liu, Internal short circuit of lithium metal batteries under mechanical abuse, Int. J. Mech. Sci. 245 (2023) 108130.

[57] H. Wang, Y. Pan, X. Liu, Y. Cao, Y. Liu, X. Zhang, Y. Mao, B. Liu, Criteria and design guidance for lithium-ion battery safety from a material perspective, J. Mater. Chem. A 10 (12) (2022) 6538–6550.
[58] W. Huang, X. Feng, Y. Pan, C. Jin, J. Sun, J. Yao, H. Wang, C. Xu, F. Jiang, M. Ouyang, Early warning of battery failure based on venting signal, J. Energy Storage 59 (2023) 106536.
[59] S. Chen, X. Wei, G. Zhang, X. Wang, X. Feng, H. Dai, M. Ouyang, Mechanical strain signal based early warning for failure of different prismatic lithium-ion batteries, J. Power Sources 580 (2023) 233397.
[60] P. Jindal, B.S. Kumar, J. Bhattacharya, Coupled electrochemical-abuse-heat-transfer model to predict thermal runaway propagation and mitigation strategy for an EV battery module, J. Energy Storage 39 (2021) 102619.
[61] M.C. Appleberry, J.A. Kowalski, S.A. Africk, J. Mitchell, T.C. Ferree, V. Chang, V. Parekh, Z. Xu, Z. Ye, J.F. Whitacre, et al., Avoiding thermal runaway in lithium-ion batteries using ultrasound detection of early failure mechanisms, J. Power Sources 535 (2022) 231423.
[62] G. Xu, Q. Han, H. Chen, Y. Xia, Z. Liu, S. Tian, Safety warning analysis for power battery packs in electric vehicles with running data, J. Energy Storage 56 (2022) 105878.
[63] J. Xu, B. Liu, X. Wang, D. Hu, Computational model of 18650 lithium-ion battery with coupled strain rate and SOC dependencies, Appl. Energy 172 (2016) 180–189.
[64] B. Liu, S. Yin, J. Xu, Integrated computation model of lithium-ion battery subject to nail penetration, Appl. Energy 183 (2016) 278–289.
[65] B. Liu, H. Zhao, H. Yu, J. Li, J. Xu, Multiphysics computational framework for cylindrical lithium-ion batteries under mechanical abusive loading, Electrochim. Acta 256 (2017) 172–184.
[66] Y. Pan, X. Zhang, Y. Liu, H. Wang, Y. Cao, X. Liu, B. Liu, Dynamic behavior prediction of modules in crushing via FEA-DNN technique for durable battery-pack system design, Appl. Energy 322 (2022) 119527.
[67] E. López-Rubio, Improving the quality of self-organizing maps by self-intersection avoidance, IEEE Trans. Neural Netw. Learn. Syst. 24 (8) (2013) 1253–1265.
[68] X. Zhang, Y. Pan, Y. Xiong, Y. Zhang, M. Tang, W. Dai, B. Liu, L. Hou, Deep learning-based vibration stress and fatigue-life prediction of a battery-pack system, Appl. Energy 357 (2024) 122481.
[69] A. Shilton, D.T. Lai, M. Palaniswami, A division algebraic framework for multidimensional support vector regression, IEEE Trans. Syst. Man Cybern. B 40 (2) (2009) 517–528.
[70] X. Zhang, Y. Pan, J. Zhou, Z. Li, T. Liao, J. Li, Forward and reverse design of adhesive in batteries via dynamics and machine learning algorithms for enhanced mechanical safety, Reliab. Eng. Syst. Saf. (2024) 110141.
[71] D. Xu, Y. Pan, X. Zhang, W. Dai, B. Liu, Q. Shuai, Data-driven modeling and evaluation of a battery-pack system's mechanical safety against bottom cone impact, Energy (2023) 130145.
[72] J. Li, D. Zhu, C. Li, Comparative analysis of BPNN, SVR, LSTM, random forest, and LSTM-SVR for conditional simulation of non-Gaussian measured fluctuating wind pressures, Mech. Syst. Signal Process. 178 (2022) 109285.
[73] L.V. Utkin, A.V. Konstantinov, V.S. Chukanov, M.V. Kots, M.A. Ryabinin, A.A. Meldo, A weighted random survival forest, Knowl.-Based Syst. 177 (2019) 136–144.